Preprints, 10th IFAC International Symposium on
Advances in Automotive Control
Columbus, Ohio, USA, August 28-30, 2022

DC Fast Charging Optimization for Capacity Fade Minimization

C. Miller * **M. Goutham** * **X. Chen** * **S. Stockar** *

* *The Ohio State University, Columbus, OH 43210 USA (e-mail: miller.8148@osu.edu).*

Abstract: DC fast charging is a critical step to support the recharging demands of electric vehicles and increase their penetration in the market. However, compared to normal Level 1 or 2 charging, DC fast charging imposes additional battery capacity fade which can result in premature aging of the battery, reducing its useful life. This paper proposes a computationally efficient, meta-heuristic approach to optimize the charging C-Rate profile while considering battery degradation associated with not only the charging but also the expected drive cycle following charging. The battery and its degradation are modeled with a semi-empirical, physics-based approach which yields a high accuracy and is computationally efficient. The meta-heuristic approach to optimize the charge profile is first validated for a simplified case with Dynamic Programming. To demonstrate the effectiveness of the approach in attenuating the battery aging, a benchmark case with 15 minutes of constant current charging of a Lithium Iron Phosphate battery is set. A nearly 1% capacity fade improvement is obtained for a single charge-discharge cycle after charging C-Rate optimization, which would generate significant benefit over the electric vehicle life.

Keywords: Charging and refueling infrastructure; Battery management systems; Modeling and control for electric and electro-magnetic components;

1. INTRODUCTION

In 2019, the transportation sector was responsible for more than 29% of all greenhouse gas emissions in the United States, having surpassed the electric power generation sector in 2017 (Environmental Protection Agency (EPA) (2021)). Newly developed electric vehicles (EVs) have been assessed to lower life-cycle emissions by 57% to 68% for comparable internal combustion engines (ICEs) (Bieker (2021)). However, the median driving range of an ICE vehicle in 2021 was 403 miles while that of an EV was only 234 miles (Department of Energy (DOE) (2022)). In addition to the range anxiety experienced by EV adopters, the wait time to recharge the battery is also much longer than that required to refuel a conventional vehicle, resulting in reduced travel flexibility for the user.

For increased penetration in the transportation sector, EVs must provide both economical and practical benefits to customers when compared with ICE vehicles. With respect to charging time, the state-of-the-art Direct Current Fast Charging (DCFC) units can provide more than 200 miles of range in 30 minutes but input significantly high power to the battery, between 25 to 350kW (Putzig et al. (2021)). The associated charge current is large and results in higher battery temperatures, which has a great impact on battery life (Drake et al. (2015); Tomaszewska et al. (2019)). In a study conducted by the US National Renewable Energy Laboratory, a 15°C reduction in average battery temperature over the life-time of the battery was found to result in roughly a double useful battery life (Keyser et al. (2017)). Additionally, insufficient battery thermal management could result in thermal runaway if the temperature reaches a critical point, posing a hazard to the user (Patel et al. (2020)). Due to the unavoidably high C-rates required for DCFC and the associated high temperatures, an effective battery thermal management system is thus essential for the safe fast charging at various operating conditions.

While active cooling strategies have already been proposed to mitigate degradation due to heat (Xia et al. (2017)), a preemptive approach is to implement charging strategies that maintain the temperature within desired bounds during fast-charging. In this case, the battery temperature control is more active compared to the application of cooling strategies. In terms of modeling, an equivalent circuit model describing the battery's electrochemical behavior is usually combined with a thermal model that captures the heat generation and dissipation. An optimal control framework is then built to minimize a cost function related to the battery degradation (Zhang et al. (2017)). By integrating a battery aging model, it is possible to obtain a degradation aware charging profile that minimizes the degradation due to DC fast charging (Guo et al. (2015)).

However, the challenge is that, the resulting optimal control problem (OCP) formulation with an objective of achieving fast-charging while minimizing capacity fade is highly nonlinear due to the electro-thermal-aging coupling (Hu et al. (2015)). Many algorithms have been proposed to find solutions, with varying successes regarding to real-time implementability. For example, in Xu et al. (2019), Dynamic Programming (DP) resulted in a 4.6% reduction in capacity fade due to solid electrolyte interface growth over 3300 charge discharge cycles (only considering ca-

pacity fade due to charging), when compared with the constant-current (CC) charging protocol. However, considering the number of states involved and the curse of dimensionality associated with DP, the computational expense is high. Moreover, their approach minimized temperature rise and capacity fade separately, yielding the possibility of two different charge profiles that minimize respective cost functions. The OCP can also be solved using Pontryagin's Minimum Principle as described in Tang et al. (2016), where a simplified aging model is used to define a severity factor that compares the expected aging with that from a nominal current profile. This is thus dependent on the selection criteria of the nominal current profile, which varies significantly from user-to-user. Machine Learning methods have been recently investigated to minimize the capacity loss during fast charging Attia et al. (2020). While results are promising, the approach requires extensive laboratory testings to failure of batteries to ensure reliable predictions of on-board cycle-life estimation.

More computationally efficient methods have been investigated such as particle swarm optimization in Salyer et al. (2021b). Results from this multi-objective study showed fast convergence of the algorithm to a near globally-optimal solution to minimize capacity fade and charge time to achieve a desired Ahr throughput. However, this study and all other previously mentioned literature neglect the effect of driving the vehicle immediately after charging. This is a strong assumption since DCFC units are more likely to be utilized on long-distance drives, indicating a greater likelihood of immediate driving after the charge event (Zhang et al. (2015)). Additionally, since the battery degradation is a strong function of pack temperature, and DCFC causes higher battery temperatures, the expected driving behavior post-charging under a higher temperature cannot be neglected.

In this paper, the DCFC current profile is optimized considering expected future driving within the OCP, to account for the higher temperatures at the end of charging. To the best of the authors' knowledge, this is the first paper reporting an optimization strategy that accounts for battery load due to future vehicle use immediately after the charge event. The solution is firstly obtained through DP to benchmark the results obtained from a real-time capable meta-heuristic optimization algorithm. Thus, the results provide an insight into the effect of battery temperature on the overall degradation during a charging event by considering both the charge and subsequent discharge processes. When the expected driving is not considered in the OCP formulation, the results show a higher temperature at the end of charging with greater capacity fade at the end of the discharge cycle, indicating the importance of this consideration.

2. THERMALLY COUPLED, MIXED-DEGRADATION MODEL

The battery model consists of three main components, namely a 0^{th} order equivalent circuit model, a lumped thermal mass model for the temperature dynamics and a simplified degradation model for battery aging. The three components are integrated as shown in Fig. 1.

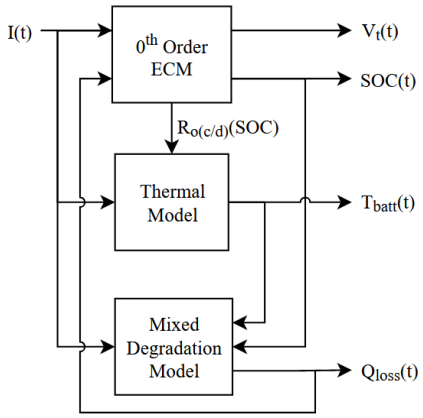

Fig. 1. Coupled Battery System Block Diagram

2.1 Equivalent Circuit Model

A 0^{th} order equivalent circuit model was utilized to model the dynamics of the battery's state of charge (SOC):

$$V_{oc}(SOC) = V_t + R_{o(c/d)}(SOC) \cdot I \tag{1}$$

$$\frac{dSOC}{dt} = \frac{I}{C \cdot 3600} \tag{2}$$

where V_{oc} is the open circuit voltage, V_t is the terminal voltage, and C is the nominal capacity of the battery in Ahr. The internal resistance and open circuit voltage in Eq. (1) are functions of the SOC and the parameters are taken from Lam et al. (2011).

2.2 Lumped Thermal Model

A simple lumped thermal mass model is developed to describe the battery temperature dynamics considering the effect of the battery current:

$$\frac{dT_{batt}}{dt} = \frac{1}{mc}(I^2 R_{o(c/d)} - hA(T_{batt} - T_{amb})) \tag{3}$$

where m is the mass of the battery pack, c is the thermal capacity, R_o is the internal resistance for charge $(_c)$ and discharge $(_d)$, h is the heat convection coefficient, A is the surface area, and T_{amb} is the ambient temperature. The values of the parameters are summarized in Tab. 1.

Table 1. Parameters for Thermal Model

Parameter	Value	Unit
m	0.07	kg
c	1100	$J/kg \cdot K$
h	5	$W/m^2 \cdot K$
A	$6.36E(-3)$	m^2

2.3 Mixed-Degradation Model

This module describes the two primary degradation mechanisms, capacity loss due to loss of active material (LAM) and capacity loss due to solid electrolyte interface (SEI) layer growth (Jin et al. (2017); Salyer et al. (2021a)):

$$Q_{SEI} = \int_0^t \frac{k_{SEI} \cdot e^{-\frac{E_{SEI}}{RT_{batt}}}}{2(1+\lambda\theta)\sqrt{t}} dt \tag{4}$$

$$Q_{LAM} = \int_0^t k_{LAM} \cdot e^{-\frac{E_{LAM}}{RT_{batt}}} \cdot SOC \cdot |I| dt \tag{5}$$

$$Q_{total} = Q_{SEI} + Q_{LAM} \tag{6}$$

where k_{SEI}, E_{SEI}, k_{LAM}, E_{LAM}, λ are calibrated parameters, and θ is the SEI layer side reaction over-potential, which is obtained by coupling an electrochemical model (Jin et al. (2017); Salyer et al. (2021a)). To reduce the computation time and model complexity for the optimization study, this paper adopts a mixed degradation model from (Miller et al. (2022)), which is based on the calibration of a lumped parameter χ as the product of λ and θ, Eq. (7):

$$\chi(SOC, T_{batt}) = \lambda \cdot \theta(SOC, T_{batt}) \tag{7}$$

To validate the implemented degradation model, battery capacity fade data for an EV with a 'complex duty cycle' was obtained from Safari and Delacourt (2011) for a 2.3 Ah LFP battery from A123 Systems (26650). The battery was charged up to 100%, held for a rest period, and discharged using this duty cycle. The cycle was repeated to yield a one-year capacity fade profile. The imposed current profile, together with a comparison between model results and original data are shown in Fig. 2, which shows a good validation of the degradation model. With modeling for one year, the capacity fade is 6.58% and the data shows a 7.57% fade.

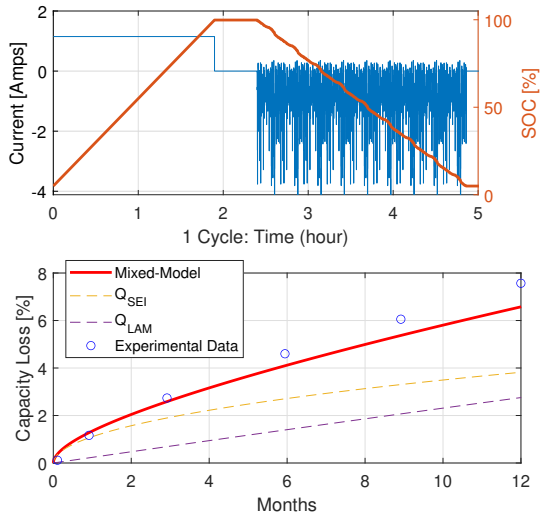

Fig. 2. One year mixed-degradation model validation from Safari and Delacourt (2011)

3. OPTIMIZATION OF CHARGING PROFILE

3.1 Optimization Problem Formulation

This paper aims to optimize a charging profile $u(t)$ defined in C-rate, such that the capacity fade of the battery is minimized over both a charge and subsequent discharge cycle, subject to state and input constraints:

$$\begin{aligned} \min_u J(x,u,w) &= \int_0^{t_f} Q_{total}(x,u,w)dt \\ \text{s.t.} \quad \dot{x} &= f(x,u) \\ x_{min} \le x(t) &\le x_{max} \\ 0 \le u(t) &\le u_{max} \\ w(t) = 0 \quad \forall \quad 0 < t &\le t_{ch} \\ u(t) = 0 \quad \forall \quad t_{ch} < t &\le t_f \end{aligned} \tag{8}$$

where x is the state vector $x = [SOC\ T_{batt}\ Q_{SEI}\ Q_{LAM}]^T$; $f(x,u)$ defines the state dynamics; and $w(t)$ is the external input vector which defines the discharge current while driving. The total time, t_f, is a fixed time that includes both charging, t_{ch}, and driving time, $t_f - t_{ch}$. The charging time is also fixed in this problem. With this definition of control input and external input, the state of charge equation in Eq. (2) becomes:

$$\frac{dSOC}{dt} = \frac{(u(t) + w(t))}{3600} \tag{9}$$

The constraints on state variables are based on A123 Systems, High Power Lithium Ion ANR26650:

$$\begin{aligned} SOC_0 \le SOC(t) \le SOC_f \\ T_{batt,min} \le T_{batt}(t) \le T_{batt,max} \end{aligned} \tag{10}$$

Moreover, at the end of the charging event at time t_{ch}, the battery must be at the required SOC:

$$SOC(t_{ch}) = SOC_f \tag{11}$$

Finally, an algebraic constraint is introduced on the terminal voltage $V_t(t)$ based on the battery specifications:

$$V_{t,min} \le V_t(t) \le V_{t,max} \tag{12}$$

Due to the nonlinearities in the optimization problem above, a possible solution approach is based on Dynamic Programming (Bertsekas (2012)). However, due to the size of the state vector, DP is computationally prohibitive for online implementation Xu et al. (2019). Moreover, splitting the battery current into a controllable profile $u(t)$ and an external input $w(t)$ makes the DP challenging to implement without further increasing the number of states. For this reason, a meta-heuristic optimization technique, particle swarm optimization (PSO), is implemented to find a near optimal solution with reduced computation time (Eberhart and Kennedy (1995)).

3.2 PSO Implementation

Particle swarm optimization is a population-based meta-heuristic algorithm where the position of each particle in the swarm is a potential solution to the optimization problem. The population or swarm of particles is initialized with positions randomly assigned throughout the feasible search space and the cost associated with the position of each particle is computed. Assuming a minimization objective, the cost associated with the position of each particle is saved as the 'personal best' solution for that particle while for the entire swarm, the solution with the minimum cost is saved as the 'global best' solution. The position and associated cost of each particle is updated at every iteration, based on a velocity equation that is a function of the personal and global best solution. The exploration through the search space continues for a defined maximum number of iterations, or until convergence.

For 2^m time-steps required for DCFC, the C-rate $u(t)$ is optimized over a 2^m dimensional search space. To ensure that the battery is charged up to the defined SOC_f, $\bar{u}_{cc}$ which is the constant C-rate required to charge up is first calculated. Then sequentially, the constant C-rate is repeatedly discretized temporally into two, while maintaining the average current to be $\bar{u}_{cc}$ over the available time.

At the first discretization step, two C-rates $u_p(1)$ and $u_p(2)$ must be obtained that have a mean current of $\bar{u}_{cc}$. This is as defined by Eq. (13) where SOC_0 is the initial SOC, in decimals and t_{Ch} is the available charging time in hours.

$$\bar{u}_{cc} = \frac{SOC_f - SOC_0}{t_{Ch}} = \frac{u_p(1) + u_p(2)}{2} \tag{13}$$

This constraint is implemented within a 1D PSO exploration of the first discretization, by defining the particle position x_p as the deviation from $\bar{u}_{cc}$, yielding C-rates $u_p(1)$ and $u_p(2)$ as obtained in Eq. (14, 15). These C-rates contribute to the Q_{total} which is the integrand of the cost function used in the PSO.

$$u_p(1) = \bar{u}_{cc} + x_p \quad \text{and} \quad u_p(2) = \bar{u}_{cc} - x_p \tag{14}$$

$$-\bar{u}_{cc} \leq x_p \leq u_{max} - \bar{u}_{cc} \tag{15}$$

The update equations of the PSO are defined by Eq. (16-17) where tunable parameters of the algorithm are the inertial weight b and acceleration coefficients c_1 and c_2. Random numbers $r_1, r_2 \in [0, 1]$ perform the stochastic aspect of the exploration, k is the iteration number, p is the particle identity and α is the relaxation factor.

$$v_p^{k+1} = bv_p^k + c_1 r_1(pbest_p - x_p^k) + c_2 r_2(gbest_p - x_p^k) \tag{16}$$

$$x_p^{k+1} = x_p^k + \alpha x_p^{k+1} \tag{17}$$

After the exploration of the search space at the first discretization step, the optimal deviation x_* is found by the 1D PSO and the resulting charge profile is composed of $u_*^{1D}(1)$ and $u_*^{1D}(2)$ as illustrated in Fig. 3.

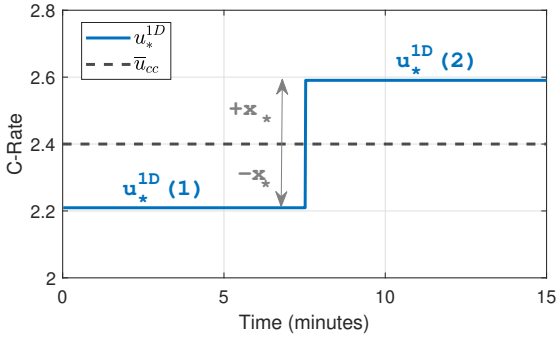

Fig. 3. 1-D PSO Optimal Solution

To discretize further and obtain a 4 time-step C-rate profile that maintains $\bar{u}_{cc}$ as the overall average current, the first two time-steps and last two time-steps must average $u_*^{1D}(1)$ and $u_*^{1D}(2)$ respectively. This is achieved by a 2D PSO where the particle position is associated with $x_p(1)$ and $x_p(2)$ which are the respective deviations from $u_*^{1D}(1)$ and $u_*^{1D}(2)$ as described by Eq. (18-21). Once the PSO finds the optimal position denoted by x_*, the 4 step current profile is given by $u*^{4D}$ as illustrated in Fig. 4

$$u_p(1) = u_*^{1D}(1) + x_p(1) \quad \text{and} \quad u_p(2) = u_*^{1D}(1) - x_p(1) \tag{18}$$

$$u_p(3) = u_*^{1D}(2) + x_p(2) \quad \text{and} \quad u_p(4) = u_*^{1D}(2) - x_p(2) \tag{19}$$

$$-u_*^{1D}(1) \leq x_p(1) \leq u_{max} - u_*^{1D}(1) \tag{20}$$

$$-u_*^{1D}(2) \leq x_p(2) \leq u_{max} - u_*^{1D}(2) \tag{21}$$

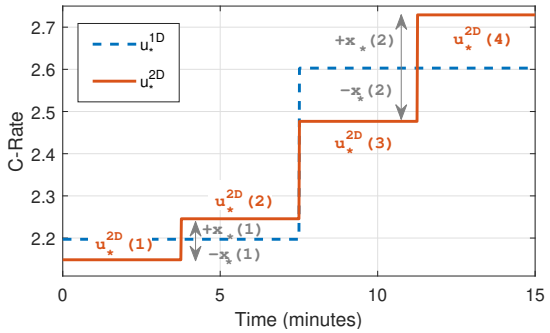

Fig. 4. 2-D PSO Optimal Solution

This approach of increasing discretization by repeatedly doubling the time-steps can be continued until the desired number of discretized time-steps is reached. Thus, 1D, 2D, 4D, ... , 2^{m-1}D PSOs are performed sequentially to arrive at the C-rates for the 2^m time-steps. At each new PSO formulation, the overall average current is maintained to be $\bar{u}_{cc}$ with the discretization rule for the ND PSO summarized in Eq. (22).

$$\frac{u_*^{2ND}(2n-1) + u_*^{2ND}(2n)}{2} = u_*^{ND}(n); \qquad for \quad n = [1:N] \tag{22}$$

In this example, discretization up to 8 time-steps was desired, and so 1D, 2D and 4D PSOs were run and the final solution is illustrated in Fig. 5.

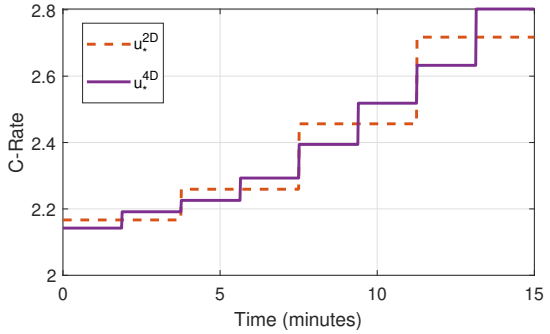

Fig. 5. 4-D PSO Optimal Solution

For a simplified case without considering the discharge cycle, the C-rate profile obtained from the PSO algorithm is compared against that from the DP algorithm described in Sundstrom and Guzzella (2009). The solutions are shown in Fig. 6, where the overall shape of the charge profiles are similar between the two algorithms, with a root mean square deviation of 0.57 and total Q_{loss} listed in Table 2. The difference in resulting solutions may be attributed to the metaheuristic nature of the PSO and the discretization of the DP algorithm used. Additionally, this DP algorithm interpolates for state variable positions and uses a backward recursion approach while the PSO simulates forward.

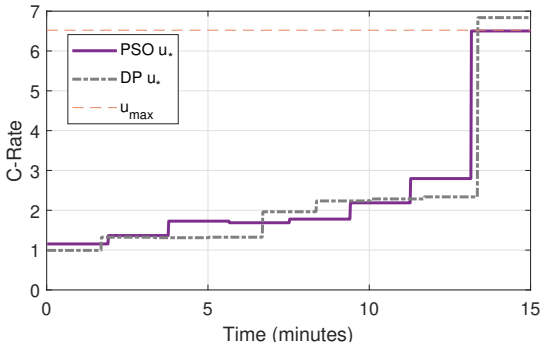

Fig. 6. PSO Validation vs Optimal DP Solution

Table 2. DP vs PSO Computation

	Computation Time	Q_{loss}
DP	3 Hours	0.019%
PSO	3 Minutes	0.020%

4. RESULTS

Following the optimization steps prescribed earlier, an 8-step charging profile was obtained for a 15-minute DC fast charge (20% to 80% SOC) initialized at 25°C followed by a complex EV duty cycle discharge (to 20% SOC). The obtained charging profile is compared with a baseline policy that uses constant-current in Fig. 7, which also shows the battery temperature during charging and discharging. The total capacity fade after the optimized charge-discharge cycle was found to be 0.1015% while that for the baseline was found to be 0.1022% over a single cycle.

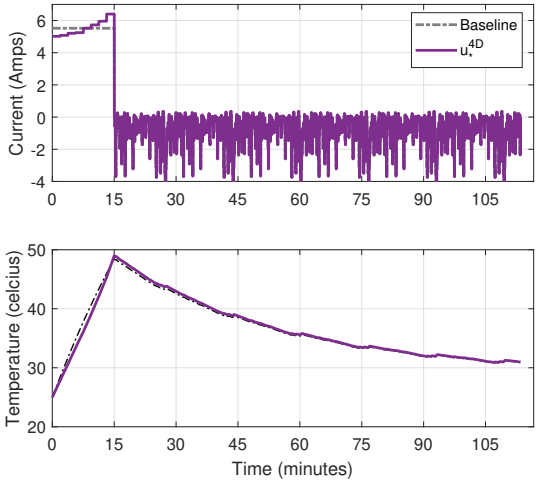

Fig. 7. Optimal Charging Policy and Temperature with Discharge Considered in Optimization

To evaluate the importance of considering the driving load immediately after DCFC, another study was conducted in which only the charging profile was optimized (the discharge was not included in optimization). The resulting optimized charge policy left the battery 12°C hotter than in the previously studied charge policy that accounted for future discharge. This is shown in Fig. 8 and the resulting capacity fade of the battery from this policy was 0.1362% compared to that of the baseline constant-current policy of only 0.1022% over just one cycle.

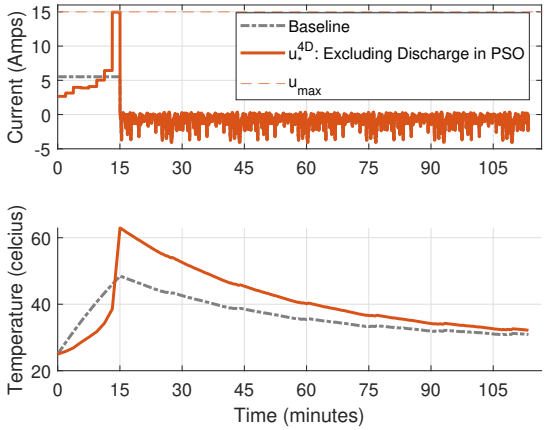

Fig. 8. Optimal Charging Policy and Temperature without Discharge Considered in Optimization

One of the primary mechanisms of degradation is capacity loss due to SEI layer growth, which is greater when the battery is held at a high SOC. Therefore, keeping the battery at a lower SOC for a longer period would be advantageous to limit capacity fade, as seen in the profiles obtained from the PSO. Additionally, temperature also plays a significant role in capacity loss, both in the loss of active material and in the SEI layer growth by affecting the reaction rate multiplied with k_{SEI} and k_{LAM}. This explains why the optimized profiles do not impose larger C-Rates on the battery which would yield larger temperatures.

It is also of interest to evaluate how the optimized charge policy evolves over extended simulations because the capacity loss due to SEI layer growth contributes lesser to the total capacity loss as the battery ages (Salyer et al. (2021a); Jin et al. (2017); Safari and Delacourt (2011)). With a battery starting at 0% capacity fade, the charge-discharge cycle of the initial study was repeated 100 times, where the PSO optimization of charging was repeated every 10 cycles. This result is shown in Fig. 9.

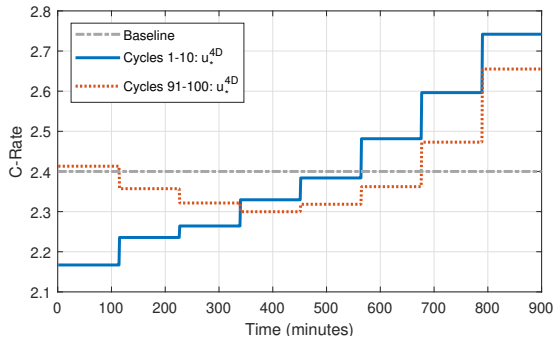

Fig. 9. Evolution of Optimal Charging Profile as the Influence of Q_{SEI} Decreases

It is clear that at charging sessions in later battery life the optimal policy limits the amount of battery temperature rise (due to high C-Rate) rather than limiting time at high SOC given that Q_{LAM} becomes the dominant loss mechanism in Q_{total}. The result tends to yield a charge profile increasingly similar to a constant-current charge

profile and it can be assumed that this trend will continue as time goes on.

5. CONCLUSIONS

In this paper, a PSO algorithm was used to optimize a discrete-step DCFC current profile, such that the battery capacity fade was minimized. The capacity fade due to an expected drive cycle immediately after charging was imposed as an additional cost in the objective function to mimic realistic charging and driving conditions. The results of the PSO algorithm showed a decrease in overall capacity fade compared to the baseline CC profile and was computationally efficient enough to be solved in real time. Future work will include the use of data driven methods to generate synthetic current profiles for the driving portion of the optimization problem.

REFERENCES

Attia, P.M., Grover, A., Jin, N., Severson, K.A., Markov, T.M., Liao, Y.H., Chen, M.H., Cheong, B., Perkins, N., Yang, Z., et al. (2020). Closed-loop optimization of fast-charging protocols for batteries with machine learning. *Nature*, 578(7795), 397–402.

Bertsekas, D. (2012). *Dynamic programming and optimal control: Volume I*, volume 1. Athena scientific.

Bieker, G. (2021). A global comparison of the life-cycle greenhouse gas emissions of combustion engine and electric passenger cars. *communications*, 49(30), 847129–102.

Department of Energy (DOE) (2022). FOTW#1221 Model year 2021 all-electric vehicles had a median driving range about 60% that of gasoline powered vehicles. https://www.energy.gov/eere/vehicles/articles/fotw-1221-january-17-2022-model-year-2021-all-electric-vehicles-had-median.

Drake, S., Martin, M., Wetz, D., Ostanek, J., Miller, S., Heinzel, J., and Jain, A. (2015). Heat generation rate measurement in a li-ion cell at large c-rates through temperature and heat flux measurements. *Journal of Power Sources*, 285, 266–273.

Eberhart, R. and Kennedy, J. (1995). A new optimizer using particle swarm theory. mhs'95. In *Proceedings of the sixth international symposium on micro machine and human science*, volume 1, 39–43. Ieee Piscataway, NJ, USA.

Environmental Protection Agency (EPA) (2021). Inventory of US Greenhouse Gas Emissions and Sinks, 1990-2019. Technical report, US Environmental Protection Agency, https://www.epa.gov/ghgemissions/us-greenhouse-gas-inventory-report-archive.

Guo, Z., Liaw, B.Y., Qiu, X., Gao, L., and Zhang, C. (2015). Optimal charging method for lithium ion batteries using a universal voltage protocol accommodating aging. *Journal of Power Sources*, 274, 957–964.

Hu, X., Perez, H.E., and Moura, S.J. (2015). Battery charge control with an electro-thermal-aging coupling. In *Dynamic Systems and Control Conference*, volume 57243, V001T13A002. American Society of Mechanical Engineers.

Jin, X., Vora, A., Hoshing, V., Saha, T., Shaver, G., García, R.E., Wasynczuk, O., and Varigonda, S. (2017). Physically-based reduced-order capacity loss model for graphite anodes in li-ion battery cells. *Journal of Power Sources*, 342, 750–761.

Keyser, M., Pesaran, A., Li, Q., Santhanagopalan, S., Smith, K., Wood, E., Ahmed, S., Bloom, I., Dufek, E., Shirk, M., et al. (2017). Enabling fast charging–battery thermal considerations. *Journal of Power Sources*, 367, 228–236.

Lam, L., Bauer, P., and Kelder, E. (2011). A practical circuit-based model for li-ion battery cells in electric vehicle applications. In *2011 IEEE 33rd International Telecommunications Energy Conference (INTELEC)*, 1–9. IEEE.

Miller, C., Goutham, M., Chen, X., Hanumalagutti, P.D., Blaser, R., and Stockar, S. (2022). A semi empirical approach to a physically based aging model for home energy management systems. URL `https://arxiv.org/abs/2206.06158`.

Patel, D., Robinson, J.B., Ball, S., Brett, D.J., and Shearing, P.R. (2020). Thermal runaway of a li-ion battery studied by combined arc and multi-length scale x-ray ct. *Journal of The Electrochemical Society*, 167(9), 090511.

Putzig, M., Bennett, J., Brown, A., Lommele, S., and Bopp, K. (2021). Electric vehicle basics. Technical report, National Renewable Energy Lab.(NREL), Golden, CO (United States).

Safari, M. and Delacourt, C. (2011). Aging of a commercial graphite/lifepo4 cell. *Journal of The Electrochemical Society*, 158(10), A1123.

Salyer, Z., D'Arpino, M., and Canova, M. (2021a). Extended physics-based reduced-order capacity fade model for lithium-ion battery cells. *ASME Letters in Dynamic Systems and Control*, 1(4).

Salyer, Z., D'Arpino, M., Canova, M., and Guezennec, Y. (2021b). Optimal health-conscious fast charging of lithium ion batteries. *IFAC-PapersOnLine*, 54(20), 516–521.

Sundstrom, O. and Guzzella, L. (2009). A generic dynamic programming matlab function. In *2009 IEEE control applications,(CCA) & intelligent control,(ISIC)*, 1625–1630. IEEE.

Tang, L., Rizzoni, G., and Cordoba-Arenas, A. (2016). Battery life extending charging strategy for plug-in hybrid electric vehicles and battery electric vehicles. *IFAC-PapersOnLine*, 49(11), 70–76.

Tomaszewska, A., Chu, Z., Feng, X., O'Kane, S., Liu, X., Chen, J., Ji, C., Endler, E., Li, R., Liu, L., et al. (2019). Lithium-ion battery fast charging: A review. *ETransportation*, 1, 100011.

Xia, G., Cao, L., and Bi, G. (2017). A review on battery thermal management in electric vehicle application. *Journal of power sources*, 367, 90–105.

Xu, M., Wang, R., Zhao, P., and Wang, X. (2019). Fast charging optimization for lithium-ion batteries based on dynamic programming algorithm and electrochemical-thermal-capacity fade coupled model. *Journal of Power Sources*, 438, 227015.

Zhang, C., Jiang, J., Gao, Y., Zhang, W., Liu, Q., and Hu, X. (2017). Charging optimization in lithium-ion batteries based on temperature rise and charge time. *Applied energy*, 194, 569–577.

Zhang, L., Shaffer, B., Brown, T., and Samuelsen, G.S. (2015). The optimization of dc fast charging deployment in california. *Applied energy*, 157, 111–122.